Original Study

OPEN

OpenEar Image Data Enables Case Variation in High Fidelity Virtual Reality Ear Surgery

*Daniel Manuel Sieber, †Steven Arild Wuyts Andersen, †Mads Sølvsten Sørensen, and ‡Peter Trier Mikkelsen

*MED-EL Elektromedizinische Geräte GesmbH, Innsbruck, Austria; †Department of Otorhinolaryngology, Rigshospitalet, University of Copenhagen, Copenhagen; and ‡Alexandra Instituttet, Aarhus, Denmark

Background: Virtual reality (VR) simulation is an established option for temporal bone surgical training. Most VR simulators are based on computed tomography imaging, whereas the Visible Ear Simulator (VES) is based on high-fidelity cryosections of a single temporal bone specimen. Recently published OpenEar datasets combine cone-beam computed tomography (CBCT) and micro-slicing to achieve similar model quality. This study explores integration of OpenEar datasets into VES to enable case variation in simulation with implications for patient-specific modeling based on CBCT.

Methods: The OpenEar dataset consists of segmented, coregistered, multimodal imaging sets of human temporal bones. We derived drillable bone segments from the dataset as well as triangulated surface models of critical structures such as facial nerve or dura. Realistic visualization was achieved using coloring from micro-slicing, custom tinting, and texture maps. Resulting models were validated by clinical experts.

Results: Six of the eight OpenEar datasets could be integrated in VES complete with instructional guides for various temporal bone surgical procedures. Resulting models were of high quality because of postprocessing steps taken to increase realism including colorization and imaging artifact removal. Bone artifacts were common in CBCT, resulting in dehiscences that most often could not be found in the ground truth micro-slicing data.

Conclusion: New anatomy models are included in VES version 3.5 freeware and provide case variation for training which could help trainees to learn more quickly and transferably under variable practice conditions. The use of CBCT for VR simulation models without postprocessing results in bone artifacts, which should be considered when using clinical imaging for patient-specific simulation, surgical rehearsal, and planning. **Key Words:** 3D modeling—Patient-specific simulation—Postprocessing—Temporal bone surgical training—Virtual reality simulation.

Otol Neurotol **42:**1245–1252, 2021.

Surgery of the human temporal bone requires a high level of understanding with regards to the three-dimensional location of anatomical landmarks and important neural and vascular structures (1). Training of novice surgeons still relies heavily on dissection of cadaveric specimens despite challenges to provide enough temporal bones in many centers (2). Surgical simulators can be an important addition to the early-stage cadaveric training of novice surgeons in temporal bone labs. It is well documented that temporal bone simulators can improve the technical skills of trainees and optimize the potential and efficiency of cadaveric training (3). However, patient-specific simulation (4) for the more experienced surgeons rehearsing and planning in complicated cases may imply higher requirements of realism and quality in simulation.

Most surgical simulators are based on medium resolution grayscale image data from clinical computed tomography (CT) (5), which provides no anatomical color information nor detailed geometry information on the more delicate bony or soft tissue structures such as the ossicles or the tympanic membrane. This low level of graphic fidelity can be a major hurdle in creating realistic and immersive virtual reality (VR) environments for surgical training and planning.

Address correspondence and reprint requests to Daniel Manuel Sieber, Dipl.-Ing. MED-EL Elektromedizinische Geräte GesmbH, Electrodes/Surgical Research and Development, Fürstenweg 77A, A-6020 Innsbruck, Austria; E-mail: daniel.sieber@medel.com

Dr. S.A.W.A. has received a postdoc grant by the Independent Research Fund Denmark (8026-00003B). The Visible Ear Simulator is developed with support from Oticon Medical, MED-EL, and the Oticon Foundation. The other authors disclose no conflicts of interest.

Supplemental digital content is available in the text.

DOI: 10.1097/MAO.0000000000003175

A stack of high-fidelity digital image data (6) resulting from a laborious cryosection process was used in the development of the Visible Ear Simulator (VES) freeware (7). The quality and realism of this anatomical model is higher, but the amount of work needed for manual segmenting and rendering has yielded only a single anatomy. This is a common concern among teachers and trainees because experience from practicing on multiple anatomies (i.e., case variation) is generally considered to be important (8).

The recently published OpenEar dataset (9) used clinical cone-beam CT (CBCT) and high-resolution CBCT in combination with anatomical micro-slicing to increase accuracy and efficacy in segmentation and to achieve a similar visual quality as the Visible Ear three-dimensional (3D) model using a less laborious process. We hypothesize that we could apply these datasets to provide additional high-fidelity virtual reality models for temporal bone surgical training.

METHODS

Data Summary

The OpenEar dataset consists of eight digitized adult human temporal bones available for free download from the Zenodo OpenData repository (9). Each dataset in the series is based on a coregistered multimodal imaging set, including clinical type CBCT of the entire temporal bone and high-resolution CBCT, as well as micro-slicing of a cropped specimen as shown in Figure 1 (left). Segmentations (i.e., delineations) of scala tympani, scala vestibuli, malleus, incus, stapes, tympanic membrane, facial nerve, chorda tympani, cochleovestibular nerve, sigmoid sinus/dura, and carotid artery are provided.

VR Simulator

The VES freeware, first published in 2009, has evolved over several iterations technologically, didactically, and in relation to the source data material: The first versions (1.0 through 1.3) focused entirely on the Visible Ear dataset (6) whereas version 2.0 introduced a modular software concept that allowed developers to load models based on other datasets into the simulator. In this article, we present the integration of the OpenEar datasets (9) in the newest version 3.5 (10) that has a fully modular system, allowing for the user's creation of training scenarios and tutorials as well as user addition of new anatomies.

Data Requirements: Drillable Bone Segment

To integrate new anatomies such as the OpenEar library into the VES, the drillable osseous segment of the temporal bone must be available as a 3D, isotropic voxel model at a high resolution of 0.2 mm or better. For a realistic simulation, two models work in concert: a central processing unit based haptic bone model, which allows physical simulation of drilling through interaction with the user input from a haptic device, and a corresponding graphics processing unit based model, which provides 3D imaging and advanced optical effects like subsurface scattering. Through precise coregistration, the two models are aligned to ensure that the physical and visual models interact properly.

Data Acquisition and Processing: Drillable Bone Segment Voxel Pipeline

CBCT data from the OpenEar library was resampled to an isometric voxel size of 0.15 mm using the Fiji software (11) setting the resolution 25% higher compared with the original Visible Ear dataset to provide more anatomical detail. A transfer function was applied in 3DSlicer (12) to remove noise and artifacts from the scans, identify bone voxels through a Hounsfield threshold limit, and adjust the Hounsfield dynamic range to match that of VES. A custom software tool was created to apply slight Gaussian filtering to achieve smooth surfaces. Tissue density values for haptic simulation in the simulator were also based on CBCT Hounsfield scale data.

Color data for each bone voxel was derived from the micro-slicing datasets of the OpenEar library. These datasets are originally anisotropic due to the nature of the micro-slicing process yielding higher in-slice resolution compared with the slice-to-slice resolution. Therefore, these were resampled to an isometric resolution. To accommodate the differences in size of the CBCT and micro-slicing datasets, a simple algorithm was created to sample colors in the micro-slicing dataset and achieve realistic color variation in the remaining bone in the model.

For manual postprocessing in relation to bony defects, a ''voxel spray'' tool was introduced into VES which can be used to fill artifactual bony voids manually where needed.

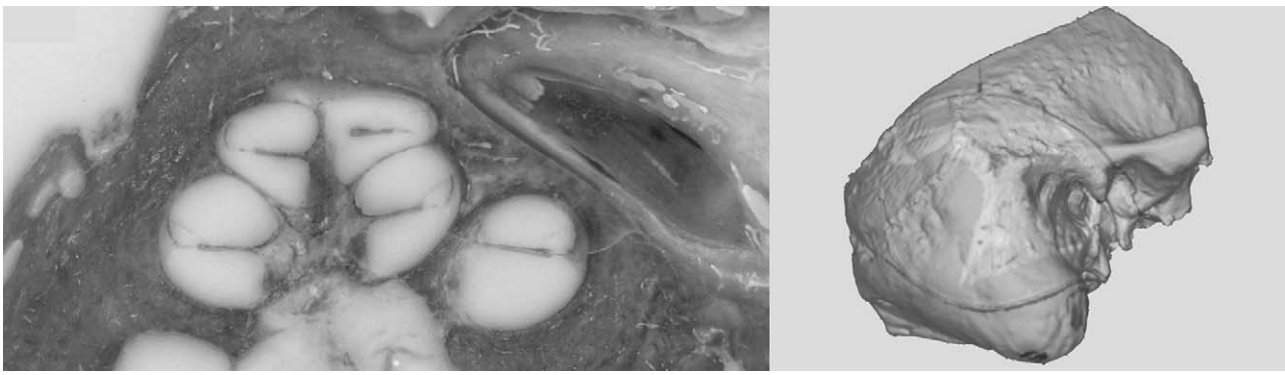

FIG. 1. Left: An example of the OpenEar dataset (Delta) showing the embedded specimen. Note the level of detail and color representation in the micro-slicing data as well as the cochlear compartments, modiolus, and osseous spiral lamina being clearly visible. *Right*: 3D reconstruction of the full dataset in the Visible Ear Simulator for surgical training. The embedded part from micro-slicing is highlighted.

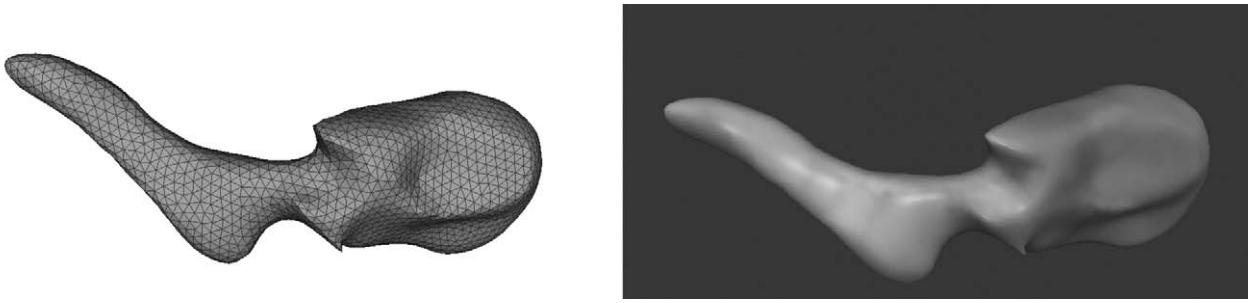

FIG. 2. An example of modeling based on segmentation of the temporal bone structures. Malleus after MeshLab processing (*left*) and after vertex colorization (*right*).

Data Processing of Nondrillable Segments: Triangulated Segments Pipeline

Manual segmentations of critical structure segments (nerves, blood vessels, dura) from the OpenEar dataset were exported as triangulated surface models. Surface normals were computed for all surfaces, and geometric decimation was applied to reduce the number of polygons in some segments which yielded models that could not be handled efficiently. Resulting surface models needed to be free of CBCT artifacts (13) such as holes, internal surfaces, nonmanifold geometries, and inverted surface normals for the sake of realism and to avoid problems in the physics simulation (e.g., contact detection between drill and anatomical segment). Therefore, new high-fidelity triangulation meshes with a defined number of elements and a uniform triangle size were created to optimize the models for fast real-time physics simulation using the Graphite software tool (14). Meshmixer (15) was used to repair remaining defects in the models, such as noisy surface patches. Meshlab (16) was used to check the resulting segments and fix instances of inverted inner and outer surfaces, which would make the use of segments in physics simulations impossible.

For the graphical model, additional color maps were created. In the middle ear ossicles each vertex of the surface triangulation was assigned the corresponding color value from the micro-slicing dataset (Fig. 2). Nonbony segments such as the dura and facial nerve were colored using UV mapping—a computer graphics method to project 2D images onto 3D models. This required the surface of the 3D object being UV unwrapped (i.e., a 2D parametrization of the 3D model). A commercial software package (17) was used to produce the UV maps for the larger models. Color for each element was determined by using a search position 0.05 mm inside the segment element surface normal to avoid artifacts caused by the micro-slicing embedding resin.

To further enhance the graphic realism of the data, textures were applied with manual painting of blood vessels on the facial nerve and dura segments (Fig. 3, right) using Blender software (18). This enhancement is considered important because the vascular pattern on these structures visible through a thin layer of bone can be a visual cue, e.g., during posterior tympanotomy drilling. Such optical surface information is always lost even in micro-slicing as an inherent artifact of the sectioning, segmentation, and reconstruction, in which the reconstructed 3D surface consists of stacked pixels selected stochastically on either side of a segment border in a 2D image. Improvements of such visual cues and graphics realism in the simulation environment seem to positively impact drilling performance as illustrated in the increased average performance (adjusted for other factors) from version 1.3 to version 2.1 and 3.0 of the Visible Ear Simulator (19).

Some of the segments appeared visually flat despite colorization, pattern tinting, and manual texturization. In reality, thin segments feature translucency, but most real-time visualization calculations, such as those needed for simulation, do not support this because of performance constraints. To simulate the effect of translucency, an efficient method was developed to

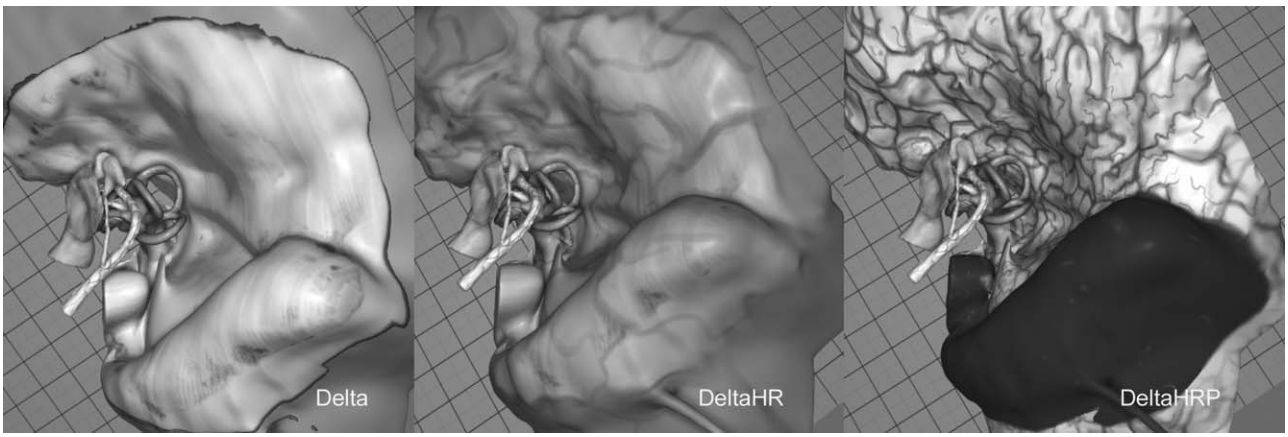

FIG. 3. Example of texture mapping to enhance realism (Delta OpenEar dataset). *Left*: UV mapping. *Middle*: Basic color tinting + minor texture. *Right*: Major texture mapping using artwork created in the Blender software.

reconstruct a view-dependent model thickness using spherical harmonics (20). To calculate these spherical harmonic coefficients (21), a signed distance field was computed representing the closest distance to a surface for every voxel, and subsequently used inside the shader to simulate translucency in real time.

The final process step in implementing the triangulated segments was the modeling of collision detection and physics. Collisions are detected using signed distance fields. The physics simulation is driven by a very simple mesh discretization using only spheres for fast intersection tests and surface skinning (22).

Validation of Visual Quality and Anatomical Validity

The resulting 3D models including the artistic enhancement of some segments were evaluated by nine experienced clinical experts from six clinics in four different countries from a viewpoint closely resembling the perspective of an operating surgeon. The experts rated the usefulness of each segment for surgical navigation for the newly implemented anatomies from the OpenEar dataset in direct comparison with the original Visible Ear dataset using a five-point Likert scale.

RESULTS

Six datasets from the OpenEar library (Delta, Epsilon, Eta, Gamma, Theta, and Zeta) were processed using the described pipeline. Datasets Alpha and Beta were not included because the quality was lower and not suited for integration. Each of the seven digital specimens (six OpenEar + one Visible Ear dataset) can now be used for training in VES—both as a left or right ear through mirroring. The current version 3.5 of the Visible Ear Simulator is available as an academic freeware from https://ves.alexandra.dk/ and will run on PCs/laptops running 64bit Microsoft Windows 7 or later and featuring a sufficiently powerful NVIDIA graphics processor (RTX2070 or better is recommended for optimal performance). A Geomagic Touch device (3D systems, Rock Hill, SC) is needed for haptic 3D control of the interactive surgical tools and for drilling with force feedback. Various tutorials for training of novice surgeons are available for each specimen with on-screen step-by-step guides for meatoplasty, cortical, and full mastoidectomy, posterior tympanotomy and CI insertion, front-to-back attico-antro-mastoidectomy, and translabyrinthine as well as fossa media approaches to the inner auditory canal. Learning support functions include transparency and slicing to ''see into the bone,'' collision warnings, optional color-coding of bone volumes to be removed (simulator-integrated tutor-function) corresponding to the step-by-step guides, and even haptic guidance of CI electrode handling.

For the integrated OpenEar datasets, the bone segment geometry of the virtual temporal bones was created from the clinical CBCT dataset, which has a large field-of-view. This allows simulation of, e.g., a full mastoidectomy and cochlear implant bed creation. For the core part of the temporal bone for which color data from micro-slicing was available (i.e., the embedded specimen), the bone volume is colored according to the respective micro-slicing colors (Fig. 1, left). This includes the mastoid, external ear canal, tympanic cavity, middle ear ossicles, and round window niche. These structures will therefore closely resemble the colors found in an actual cadaveric temporal bone. For the voxels outside of the micro-slicing dataset, the CBCT bone volume was manually colored (Fig. 1, right). The authors have made resulting UV maps as well as 3D models including vertex coloring available for the Delta dataset as a sample (23).

The authors also evaluated the fidelity of each of the VR models and frequently observed bone voxel defects in the 3D models (Table 1), imitating for example a dehiscence at the horizontal or vertical segment of the facial nerve, or bony defects at the interface with dura (Fig. 4). These defects were often less prominent using the high-resolution CBCT as source material when compared with the clinical CBCT. However, not all defects were artifacts of processing the CBCT to make 3D models: in a few cases, actual defects and dehiscences were also found in micro-slicing. For example, in the Eta dataset, a dehiscence of the superior semicircular canal was found in both the CBCT and the micro-slicing datasets; and in the Epsilon dataset, there seems to be an extensive dehiscence of the horizontal part of the facial nerve, which in the micro-slicing is merely a partial dehiscence. These examples show that it can be impossible to judge whether a bone defect is merely an artifact in CBCT imaging or an actual anatomical finding without access to ground truth imaging such as micro-slicing. For the scala tympani, several of the OpenEar models had bony voxel artifacts ''growing'' inside the scala making it difficult or impossible to insert a CI electrode in the simulator using the dataset without manual postprocessing. Finally, the CBCT models in two cases (Theta and DeltaHR) also capped the incus in an artificial layer of bone that is not a part of the structure.

The fidelity of models can be improved 1) by increasing the quality of the data acquisition (i.e., increasing scan resolution), 2) by voxel postprocessing, and 3) by using texture maps to represent blood vessels and other visual cues. The Delta dataset may serve as an example of what was done in VES version 3.5. The external surface toward the dura and the sigmoid sinus had many gross defects when the clinical CBCT dataset (0.25 mm resolution) was used for 3D modeling (Fig. 5, left). However, even at a better resolution (0.125 mm) some of these defects persisted (Fig. 5, middle). With manual postprocessing using the voxel spray tool and drilling, these defects could be corrected (Fig. 5, right) along with correction of other bony artifacts such as the incus being embedded in bone (Fig. 4, middle), a defect of the promontory wall, and bony artifacts inside scala tympani. Finally, adding texture maps (Fig. 3, middle and right) provides further realism of the simulation (Fig. 4, middle and right). These postprocessing procedures still require extensive manual labor, pushing the time to integrate a new anatomy into the simulator to 25 to 30 hours which could be optimized by automatization over time.

TABLE 1. *Fidelity of virtual reality 3D models before manual postprocessing*

		Voxel Artifacts/Defects in the 3D Model							
Source Material (Resolution)	Dataset	External Surface	Dura	Sigmoid Sinus	Labyrinth	Facial Nerve	Lateral Face of Carotid	Scala Tympani	Ossicles
Micro-slicing (50 μm)	Visible Ear	−	−	−	−	−	−	− CI electrode insertion easy	−
Clinical cone-beam CT (250 μm)	OpenEar: Theta	−	−	−	−	−	−	+ Narrow due to artifacts, CI electrode insertion difficult	+ Incus capped in some bone
	OpenEar: Zeta	−	−	−	−	−	−	++ Very narrow due to artifacts, CI electrode insertion impossible	−
	OpenEar: Gamma	−	−	−	−	+ Bone voxel defect	+ Bone voxel defect	− CI electrode insertion easy	−
	OpenEar: Eta	−	(+) Bone voxel defect in micro-slicing too	+ Bone voxel defect	(+) Bone voxel defect in micro-slicing too: SSC dehiscence in fossa media.	++ Large bone voxel defect	+ Bone voxel defect	+ Narrow due to artifacts, CI electrode insertion difficult	−
	OpenEar: Epsilon	+ Bone voxel defect	+ Bone voxel defect	−	−	+(+) Large bone voxel defect. Partial dehiscence in micro-slicing too.	−	− CI electrode insertion easy	−
	OpenEar: Delta	+ Bone voxel defect	+++ Very large bone voxel defect	+++ Very large bone voxel defect	−	++ Large bone voxel defect	++ Large bone voxel defect	+ Narrow due to artifacts, CI electrode insertion difficult	−
High-resolution cone-beam CT (125 μm)	OpenEar: Delta HR	+ Bone voxel defect	+ Bone voxel defect	+ Bone voxel defect	+ Bone voxel defect. Promontory defect inferior to the stapes footplate	+ Bone voxel defect	+ Bone voxel defect	++ Very narrow, CI electrode insertion impossible	+++ Incus embedded in bone
	OpenEar: Delta HR with post-processing	−	−	−	−	−	−	− CI electrode insertion easy	−

All artifacts were removed for final integration in VES.
− No artifacts or defects, i.e., normal anatomy in micro-slicing as well as the 3D model.
(+) Bone defect in micro-slicing as well as the 3D model.
+ Bone voxel artifact in the 3D model only.

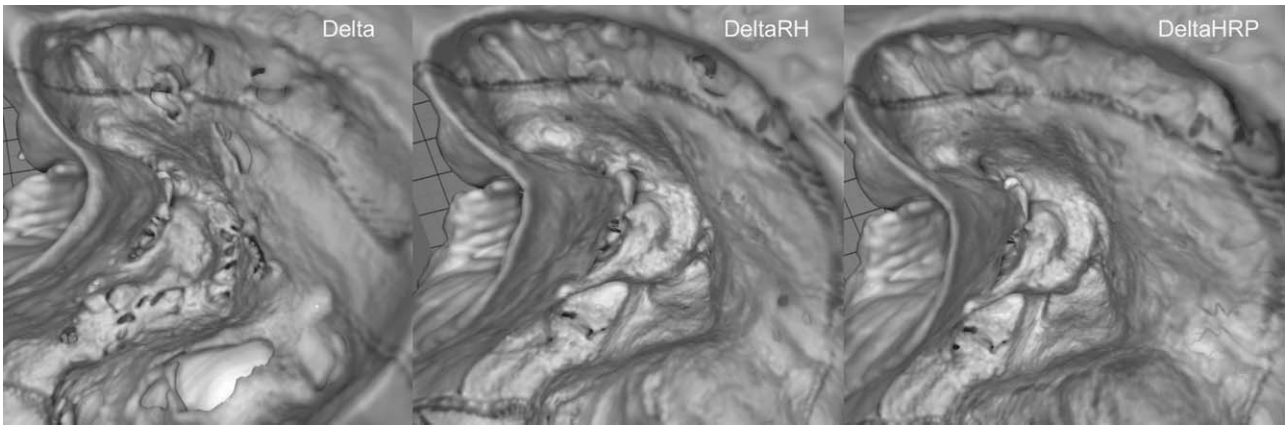

FIG. 4. Examples of how bony defects appear in the differently processed datasets of Delta during a virtual drilling of an anatomical mastoidectomy. *Left*: The clinical CBCT dataset has large artifacts observed as dehiscences at dura and sinus. *Middle*: The high-resolution CBCT dataset has smaller dehiscence artifacts but the ossicles are embedded in bone. *Right*: The manually postprocessed high-resolution dataset has no bone artifacts. CBCT indicates cone-beam computed tomography.

Ultimately all artifacts mentioned in Table 1 and beyond were removed for the implementation in VES during postprocessing of all included OpenEar models. Resulting virtual models included in VES version 3.5 provide the highest quality of models for training (i.e., similar to the DeltaHRP in Fig. 5) approaching a similar visual quality as compared with the original Visible Ear models. Nonetheless, to demonstrate the challenges and effects of imaging and postprocessing on fidelity and realism, all three Delta models (i.e., based on the clinical CBCT, high-resolution CBCT, and high-resolution CBCT with manual postprocessing) are available in VES 3.5. The expert evaluation of the OpenEar models revealed similar ratings for the OpenEar models (range avg 3.7–4.1) and the Visible Ear 3.5 models (avg 4.2). A clear improvement was found between the low-resolution Delta models (avg 3.4), high-resolution DeltaHR models (avg 3.6), and final simulator implementation including manual postprocessing DeltaHRP (avg 4.1). Questionnaire, http://links.lww.com/MAO/B262 and detailed evaluation results for individual structures are found in Supplemental Digital Content 1, http://links.lww.com/MAO/B263.

DISCUSSION

We present a process for developing high-fidelity VR simulation based on the publicly available OpenEar datasets. The aim of the OpenEar project was to develop a new method to create digital temporal bone specimens in a time-efficient way and to focus on those structures needed to adequately simulate the most common otologic procedures including middle and inner ear surgery. Even though the original Visible Ear data remains unparalleled as a complete digital representation of the human temporal bone including, e.g., brain and skin segments, the

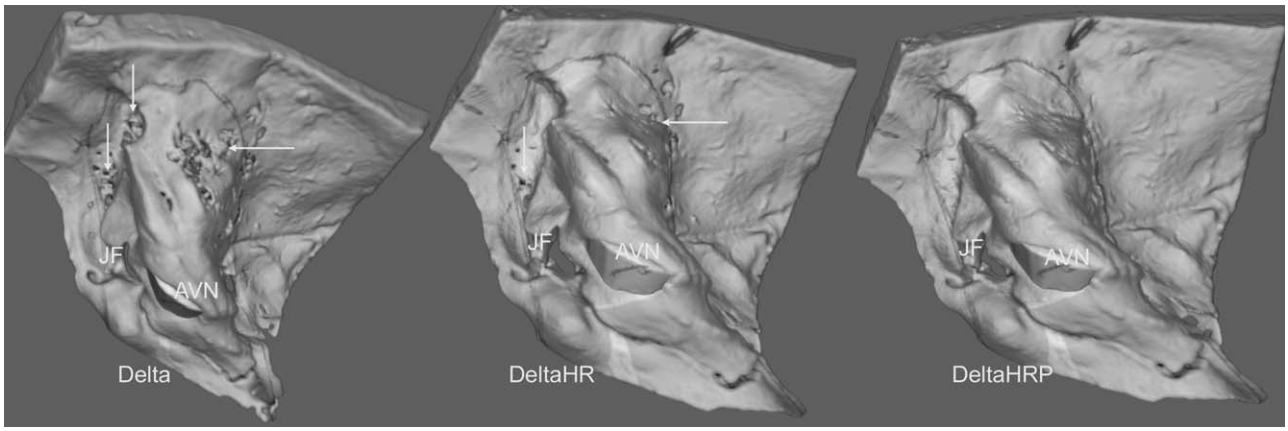

FIG. 5. Different 3D reconstructions of the OpenEar dataset (Delta). *Left*: Model based on the clinical type CBCT + automatic smoothing routines. *Middle*: Model based on the high-resolution CBCT + automatic smoothing routines. *Right*: Model based on the high-resolution CBCT + automatic smoothing routing + manual postprocessing. Arrows mark bony defects (i.e., artifacts). AVN indicates acusticovestibular nerve; CBCT, cone-beam computed tomography; JF jugular foramen.

OpenEar data has been successfully used to expand the number of anatomies in high-fidelity virtual temporal bone training. A group of international experts has evaluated the implementation of the OpenEar anatomies in the simulator and rated the new models almost as highly as the original Visible Ear models. The creation of patient-specific high-fidelity models for presurgical rehearsal and planning requires high-resolution imaging, accurate, and fast segmentation, as well as methods to warp and apply meaningful coloring to grayscale type data. While the latter could be solved in software engineering given adequate time and resources, clinically available imaging quality and segmentation methods are currently hindering advances in this field.

Two studies have investigated the use of clinical imaging for patient-specific VR simulation, with both studies based on cadaveric material: Arora et al. (24) used clinical CT and Locketz et al. (25) used clinical CBCT. Both groups report substantial need for manual interaction to achieve usable models. In a recent study (26), novice simulator users supported patient-specific simulator rehearsal before surgery. However, this recommendation was based on the drilling of a single bone rendered from microCT, which is not applicable for use in patients.

Our study further highlights that while clinical CBCT can be used to generate patient-specific models, there might be considerable defects and artifacts in the resulting 3D models. Most of these abnormalities are artifacts resulting from the acquisition, processing, and reconstruction of the data for 3D modeling and could not be found in the ground truth micro-slicing data material. However, as some of the defects represented true defects also found in the micro-slicing data, there is no clinically available way of knowing whether defects are true or artifacts from clinical CBCT imaging. Consequently, this might mislead surgeons regardless of whether standard review of the clinical imaging is done preoperatively in a clinical imaging viewer (i.e., DICOM viewer) or whether data is modeled for 3D VR visualization. The experienced surgeon will be aware of bias inherent to CBCT such as apparent dehiscences but also bias due to the reconstruction and visualization in the virtual reality environment. Manual postprocessing can of course be added, but besides being time consuming and resource intensive, this provides no guarantee of a ''truer'' representation without ground truth imaging available.

Nonetheless, 3D modeling offers advantages such as interaction with the dataset through drilling and CI electrode insertion. The manual postprocessing with closure of defects and removal of artifacts needed for a solid simulation is however still not feasible or attractive in clinical routine where time of physicians is extremely precious. We therefore propose to do this mainly when establishing a case library for temporal bone surgical training as in this study, which has made six new cases available within the latest version of VES complete with many tutorials for drilling mastoidectomy, CI insertion, and more. The simulator software is provided as academic freeware online (10).

The implementation of the OpenEar datasets represents a valuable extension of the Visible Ear Simulator capabilities, as it allows training of surgical procedures covering more anatomical variations without sacrificing some of the fundamental advantages of model colorization based on empirically obtained data. Being able to offer variability of practice could increase the learning speed in simulator training significantly when compared with constant practice (27), as it allows learners to sample a useful range of parameter-sets (in our case: anatomical variations) and observe outcomes (in our case: surgical successes or traumata) dependent on their actions. Furthermore, Huet et al. (28) found in aviation simulator participants that variable practice training may accelerate the education of attention to more useful informational variables. Translated into our application, surgical simulator trainees in constant practice settings could, e.g., depend too much on a certain anatomical landmark which is prominent in their single anatomy scenario. By adding anatomical variation and variable practice to the simulation, trainees would realize they cannot rely on this landmark only and add further landmarks into their decision-making process, improving transferability of their simulator-acquired skills. With the addition of further anatomies it is anticipated that simulations will stay attractive up to a higher number of repetitions, which may aid in internalizing the surgical procedure at an even higher level than what has been found in previous work where an apparent plateau in performance is observed after only few repetitions of training (29,30).

Even though basic surgical skills can effectively be learned using low fidelity simulation (such as for example box trainers in laparoscopy) most studies have only investigated this for novice learners (31). A high graphical realism as pursued by the Visible Ear and OpenEar models might be more important in complex procedures (32) where accurate visual cues are important and higher fidelity of the simulation is beneficial for more advanced learners (33).

Further studies using a contemporary validity framework (34) are needed to demonstrate that the positive effects of variability of practice can also be observed in temporal bone surgical simulation and to create validity evidence supporting increased fidelity of the graphics.

After more than 15 one-eared VES years, the OpenEar project has made six additional digital temporal bone datasets available to the scientific community. With the integration into the latest version 3.5 of the Visible Ear Simulator, these are now also available for surgical training in a high-fidelity surgical simulator environment for the benefit of VR training of ear surgery. The modularization of the simulator and the possibility for users to create their own tutorials could take surgical simulation to a new and community-based level. This project yielded several simple but novel solutions to technological challenges encountered in the process development as well as insights into implications of using clinical CBCT for patient-specific simulation.

REFERENCES

1. Gulya AJ, Minor LB, Glasscock ME, Poe D. *Glasscock-Shambaugh Surgery of the Ear*. Beijing, China: People's Medical Publishing House; 2010.
2. Frithioff A, Sørensen MS, Andersen SAW. European status on temporal bone training: A questionnaire study. *Eur Arch Otorhinolaryngol* 2018;275:357–63.
3. Lui JT, Hoy MY. Evaluating the effect of virtual reality temporal bone simulation on mastoidectomy performance: A meta-analysis. *Otolaryngol Head Neck Surg* 2017;156:1018–24.
4. Sethia R, Wiet GJ. Preoperative preparation for otologic surgery: Temporal bone simulation. *Curr Opin Otolaryngol Head Neck Surg* 2015;23:355–9.
5. Tolsdorff B, Petersik A, Pflesser B, et al. Individual models for virtual bone drilling in mastoid surgery. *Comput Aided Surg* 2009;14:21–7.
6. Sørensen MS, Dobrzeniecki AB, Larsen P, Frisch T, Sporring J, Darvann TA. The visible ear: A digital image library of the temporal bone. *ORL J Otorhinolaryngol Relat Spec* 2002;64:378–81.
7. Sørensen MS, Mosegaard J, Trier P. The visible ear simulator: A public pc application for gpu-accelerated haptic 3D simulation of ear surgery based on the visible ear data. *Otol Neurotol* 2009; 30:484–7.
8. Cook DA, Hamstra SJ, Brydges R, et al. Comparative effectiveness of instructional design features in simulation-based education: Systematic review and meta-analysis. *Med Teach* 2013;35: e867–e898.
9. Sieber DM, Erfurt P, John S, et al. The OpenEar library of 3D models of the human temporal bone based on computed tomography and micro-slicing. *Sci Data* 2019;6:180297.
10. The Visible Ear Simulator. Available at: https://ves.alexandra.dk. Last accessed: October 23, 2020.
11. Schindelin J, Arganda-Carreras I, Frise E, et al. Fiji: An open-source platform for biological-image analysis. *Nat Methods* 2012;9: 676–82.
12. Fedorov A, Beichel R, Kalpathy-Cramer J, et al. 3D slicer as an image computing platform for the quantitative imaging network. *Magn Reson Imaging* 2012;30:1323–41.
13. Hsieh J. *Computed Tomography: Principles, Design, Artifacts, and Recent Advances*. Bellingham, WA: SPIE Press; 2003. 183–187.
14. Institute National de Recherche en Informatique et en Automatique, Graphite Software. Available at: http://alice.loria.fr/software/graphite/. Last accessed: October 23, 2020.
15. Autodesk, Meshmixer. Available at: http://www.meshmixer.com/. Last accessed: October 23, 2020.
16. Cignoni P, Callieri M, Corsini M, Dellepiane M, Ganovelli F, Ranzuglia G. MeshLab: An open-source mesh processing tool. *Eurographics Italian Chapter Conference* 2008;129–36.
17. [3D-IO] Games & Video Production GmbH, Unwrella Software. Available at: https://www.unwrella.com/. Last accessed: October 23, 2020.
18. Blender free and open source 3D creation suite. Available at: https://www.blender.org/. Last accessed: October 23, 2020.
19. Andersen SAW, Park YS, Sørensen MS, Konge L. Reliable assessment of surgical technical skills is dependent on context: An exploration of different variables using generalizability theory. *Acad Med* 2020;95:1929–36.
20. Barré-Brisebois C, Bouchard M. GDC talk 2011 at: https://www.gdcvault.com/play/1014538/Approximating-Translucency-for-a-Fast. Last accessed: October 23, 2020.
21. Green R. Spherical Harmonic Lighting. *Sony Computer Entertainment America* 2003.
22. Mueller M, Chentanez N. Solid simulation of oriented particles. ACM Trans Graph. Siggraph, 2011;92:1–10.
23. Sieber DM, Andersen SAW, Sørensen MS, Trier P. OpenEar color example from Visible Ear Simulator anatomy Delta [Data set]. *Zenodo* 2020.
24. Arora A, Swords C, Khemani S, et al. Virtual reality case-specific rehearsal in temporal bone surgery: A preliminary evaluation. *Int J Surg* 2014;12:141–5.
25. Locketz GD, Lui JT, Chan S, et al. Anatomy-specific virtual reality simulation in temporal bone dissection: Perceived utility and impact on surgeon confidence. *Otolaryngol Head Neck Surg* 2017;156: 1142–9.
26. Compton EC, Agrawal SK, Ladak HM, et al. Assessment of a virtual reality temporal bone surgical simulator: A national face and content validity study. *J Otolaryngol Head Neck Surg* 2020;49:17.
27. Schmidt RA. A schema theory of discrete motor skill learning. *Psychol Rev* 1975;82:225–60.
28. Huet M, Jacobs DM, Camachon C, Missenard O, Gray R, Montagne G. The education of attention as explanation of variability of practice effects: Learning the final approach phase in a flight simulator. *J Exp Psychol Hum Percept Perform* 2011;37:1841–54.
29. Andersen SA, Konge L, Cayé-Thomasen P, Sørensen MS. Learning curves of virtual mastoidectomy in distributed and massed practice. *JAMA Otolaryngol Head Neck Surg* 2015;141:913–8.
30. Andersen SA, Konge L, Mikkelsen PT, Cayé-Thomasen P, Sørensen MS. Mapping the plateau of novices in virtual reality simulation training of mastoidectomy. *Laryngoscope* 2017;127: 907–14.
31. Lefor AK, Harada K, Kawahira H, Mitsuishi M. The effect of simulator fidelity on procedure skill training: A literature review. *Int J Med Educ* 2020;11:97–106.
32. Sarmah P, Voss J, Ho A, Veneziano D, Somani B. Low vs. high fidelity: The importance of 'realism' in the simulation of a stone treatment procedure. *Curr Opin Urol* 2017;27:316–22.
33. Sidhu RS, Park J, Brydges R, MacRae HM, Dubrowski A. Laboratory-based vascular anastomosis training: A randomized controlled trial evaluating the effects of bench model fidelity and level of training on skill acquisition. *J Vasc Surg* 2007;45:343–9.
34. Cook DA, Beckman TJ. Current concepts in validity and reliability for psychometric instruments: Theory and application. *Am J Med* 2006;119:166.e7–166.e16.